The Journal of Experimental Biology 207, 4543-4550
Published by The Company of Biologists 2004
doi:10.1242/jeb.01328

Anatomy of a live invertebrate revealed by manganese-enhanced Magnetic Resonance Imaging

Jens Herberholz[1,2,*], Christopher J. Mims[1], Xiaodong Zhang[2,3], Xiaoping Hu[2,3] and Donald H. Edwards[1,2]

[1]*Georgia State University, Department of Biology, Atlanta, GA 30302-4010, USA*, [2]*Center for Behavioral Neuroscience, Atlanta, GA 30302-3966, USA* and [3]*Emory University, Department of Biomedical Engineering, Atlanta, GA 30322-4600, USA*

*Author for correspondence at address 1 (e-mail: biojhh@langate.gsu.edu)

Accepted 11 October 2004

Summary

Non-invasive imaging technologies such as Magnetic Resonance Imaging (MRI) are increasingly in demand by researchers in many biological disciplines. However, when imaging small animals such as invertebrates, not only is the use of high-field magnets necessary to gain satisfactory spatial resolution, but the achievement of adequate contrast between tissues also requires the identification of applicable imaging parameters by means of expensive and time-consuming procedures. Here we report that systemically administered manganese can act as an effective MRI contrast agent for quick and non-invasive imaging of the nervous system and other complex anatomical structures in a small aquatic animal. Due to the tendency of manganese ions to differentially accumulate in most soft tissues, higher overall signal intensity and strongly improved contrast between structures yield data well suited for digital post-processing into three-dimensional models. Within a few hours this technique can efficiently generate anatomical images that are not obtainable with conventional methods, thus demonstrating a new and exciting approach to invertebrate research.

Supplementary material available online at
http://jeb.biologists.org/cgi/content/full/207/26/4543/DC1

Key words: crayfish, invertebrate, manganese, anatomy, imaging, Magnetic Resonance Imaging (MRI).

Introduction

For many biologists it has become necessary to image the anatomy of the same individual throughout embryonic or juvenile development, to compare anatomical or morphological changes induced in one animal by behavioral or pharmacological treatment, and to compare anatomical structures in different animals. In particular, studies of invertebrate model systems in developmental biology, neurobiology, physiology, genetics and other biological disciplines could be improved by imaging the anatomy of living subjects.

Magnetic Resonance Imaging (MRI) is a non-invasive method that allows the imaging of live animals. The overall signal intensity of a magnetic resonance (MR) image is primarily determined by the density as well as the longitudinal (T_1) and the transversal relaxation times (T_2) of protons in the sample. Differences in proton density (PD), T_1, and T_2 between tissues then translate into areas of different brightness in the acquired images. The combination of repetition time (T_R) and echo time (T_E) define the 'weighting' (e.g. T_1, PD, T_2) of the image, and different weightings generate the best results for specific tissues. When applying MRI to a well-studied subject, the most effective imaging parameters have usually been previously determined in the literature. Nevertheless, the identification and separation of different morphological and anatomical areas is complicated when signal differences between bordering tissues are nonexistent or low. Thus, to increase contrast between areas of interest, multiple imaging sessions at different combinations of T_R and T_E are required to differentiate soft tissues belonging to the same or different organs when applying conventional MRI (Benveniste and Blackband, 2002). Depending on the field strength of the magnet, each of these scans will take several hours to achieve the desired resolution. Unfortunately, multiple long imaging sequences jeopardize the survival of the imaged subject. Moreover, when imaging an organism for which the relaxation times of different tissues have not been previously established, the applicable MR parameters are unknown and need to be experimentally identified *via* multiple imaging sessions, a time-consuming and therefore potentially expensive undertaking.

Manganese (Mn^{2+}) is a powerful T_1-relaxation agent that positively enhances MRI signal intensity in the areas where it

has accumulated. However, the documented (neuro-) toxicity of the manganese ion makes use of a chelated form of Mn^{2+} necessary when it is used as a contrast agent in human subjects during medical examination. In contrast to its ionic form, chelated Mn^{2+} (mangafodipir trisodium, Mn-DPDP) is restricted from entering ion channels, which prevents intracellular uptake. Primarily used for imaging the liver and pancreas in humans, Mn-DPDP dechelates inside the tissue where free Mn^{2+} ions subsequently accumulate (Runge, 2000; Weinmann et al., 2003).

Recently, manganese-enhanced MRI (MEMRI) has been used to image neural activity and neuronal connections in the brains of non-human vertebrates. Due to its chemical structure, Mn^{2+} can enter depolarized cells through voltage-gated calcium channels and MEMRI therefore allows identification of active brain areas. Mn^{2+} is also transported along axons and across synapses from one neuron to the next. Neuronal circuitry has been studied after focal injections of $MnCl_2$ into specific areas of the brain (Pautler et al., 1998, 2003). Reported as an undesirable side effect in these studies, Mn^{2+} ions also accumulate in areas other than the nervous system.

The accumulation of Mn^{2+} ions in various tissues of decapod crustaceans was investigated in lobsters that had been exposed to different concentrations of Mn^{2+} in the surrounding water for several weeks. Using atomic absorption spectrophotometry, it was reported that Mn^{2+} uptake was highest in the nervous tissue, and Mn^{2+} also accumulated in the blood, gills, hepatopancreas, exoskeleton and in muscle tissue, resulting in a slight reduction in muscle performance (Baden and Neil, 1998; Baden et al., 1999).

For the first time, we now describe the ability of ionic Mn^{2+} to act as a contrast agent that differentially accumulates in most tissues, highlights otherwise undetectable structures and strongly improves contrast between organs, allowing more effective and time-efficient imaging and anatomical reconstructions.

Materials and methods

Preparation of animals and cannulae

Adult crayfish *Procambarus clarkii* Girard of both sexes (size: 9–12 cm rostrum to telson; mass 24–38 g) were cannulated in the pericardial sinus to the immediate left or right of the heart with fused silica tubing for $MnCl_2$ (Manganese [II] chloride tetra-hydrate, minimum 99%; Sigma-Aldrich; St Louis, MO, USA) injection. Each cannula was constructed of 0.25 cm of fused silica tubing (i.d. 0.2 mm; Polymicro Technologies, Phoenix, AZ, USA) inserted into 1–3 m of polythene tubing (i.d. 0.28 mm; Portex, Hythe, UK) connected to a MicroFil nonmetallic syringe needle (World Precision Instruments, Sarasota, FL, USA) on a 1 ml syringe. The volume of 1 cm of tubing was ascertained by filling a length of tubing with 10 µl of Methylene Blue dye dissolved in water and subsequent measurement of the length of tubing that appeared blue. Cannulae were then filled with the appropriate concentration of $MnCl_2$ dissolved in crayfish saline. Once filled, a small bubble was introduced at the end of the polyethylene tubing furthest from the end connected to the fused silica tubing. Subsequently, a MicroFil syringe needle was inserted into the tubing, and a 1 ml syringe filled with Methylene Blue dissolved in water was inserted into the syringe needle. In this way, an easy visual reference (the position of the Methylene Blue within the transparent tubing) could be used to determine the amount of Mn^{2+} injected.

A hole was drilled using a 27 gauge needle in the carapace of each crayfish, 1–2 mm to the left or right of the midline created by the juncture of the two branchio-cardiac grooves, posterior of the cervical groove demarcating the line where the crayfish's head and thorax are fused. Fused silica tubing, already inserted into the polyethylene tubing and the rest of the $MnCl_2$ delivering apparatus, was inserted so that only 1 mm of silica tubing penetrated the crayfish before its entry was arrested by the beginning of the polythene tubing. This juncture was then sealed with a few drops of gel superglue, and further secured with a few drops of methyl methacrylate denture material (Pearson Dental Supply, Sylmar, CA, USA).

Animals were not fed for 1 week prior to imaging in order to prevent any motion artefacts in the stomach. As a consequence, the interior of the stomach was usually filled with air during scans. Before scanning, the animals were restrained in one of two ways. For full-body scans, the crayfish were placed in 100 ml round centrifuge tubes (Nalgene, Rochester, NY, USA) and embedded in 2% liquid agarose (Type II; Sigma-Aldrich) chilled to just above its gel point (~34°C). For scans of tissues localized to the head and thorax, animals were placed in 100 ml centrifuge tubes and secured with pieces of styrofoam and a drop of hot glue on the dorsal side of the carapace. In the case of agarose embedding, crayfish were able to tolerate low-oxygen conditions for up to 8 h. In the case of restraint with styrofoam, only small amounts of water (5–10 ml) were added to the interior of the tube, to prevent dryout. Crayfish immobilized in this way survive for at least 72 h.

Imaging and application of contrast agent

All experiments were performed using a 4.7 Tesla horizontal bore (33 cm) magnet (Oxford Magnet Technology, Oxford, UK). An active shielded, 11.7 cm i.d. gradient-insert operated at a maximum of 25 G cm^{-1} and a rise time of 250 µs. The scanner was interfaced to a Unity INOVA console (Varian, Palo Alto, CA, USA). A multi-slice, spin-echo sequence was used and images were acquired by means of a quadrature birdcage radiofrequency (RF) coil (3.7 cm i.d.).

To evaluate the combination of MR parameters and dose of $MnCl_2$ for optimal contrast and signal enhancement after injection, different solutions; i.e. 10–250 µl/20–240 mmol l^{-1}, roughly adapted from experiments in rodents (Morita et al., 2002; Aoki et al., 2003), were injected into the circulation of adult crayfish. The dose of $MnCl_2$ (0.26–10.42 µl g^{-1} body mass) was adjusted in direct proportion to the mass of the experimental subject, relative to a standard animal of 26.5 g. The animals were subsequently imaged in

short sessions at different combinations of T_R (0.5–6 s) and T_E (10.2–500 ms). From these images a matrix (T_R/T_E *vs* dose of $MnCl_2$) was constructed. After the matrix was reviewed, MR parameters and Mn^{2+}-concentrations were selected for all subsequent experiments based on the following criteria: (1) overall signal intensity, (2) visibility of relevant tissues, (3) contrast between relevant tissues. The values for each experiment are given in the text or figure legend.

Lower amounts of $MnCl_2$ ($\leqslant$60 µl) were administered over the course of 1–3 min, larger amounts over 4–5 min, inside or outside the magnet. Administrations of the contrast agent inside the magnet were applied when the exact same anatomical location within the same animal needed to be compared before and after the injection. On occasion, we found that crayfish that were injected inside the magnet circulated the injected Mn^{2+} very slowly. The contrast agent pooled around the injection site, most likely because immobilized crayfish reduced their heartbeat, which prevented the Mn^{2+} from being quickly distributed throughout the body. Due to the relatively slow clearance rate of Mn^{2+} from the tissue, injections can also take place outside the magnet, in which case the cannula used for administration of the contrast agent was subsequently removed from the animal. Crayfish were then stimulated with a handheld probe to move around in a water-filled tank for 45–60 min to facilitate circulation and accumulation of Mn^{2+}.

High doses of $MnCl_2$ (>100 µl/120 mmol l^{-1}) caused detectable behavioral alterations immediately after injection (discontinuing locomotion, lowering posture, rigidity or tremor) and were not used for subsequent experiments.

A small tube (5 ml) filled with deionized water was placed as a reference in the 100 ml centrifuge tube ventral to each crayfish for normalizing the signal intensity in images acquired during different sessions.

Digital data processing

Anatomical structures were individually delineated (‘segmented’) using Amira™ v. 3.1 on a Dell PC using a combination of automated and manual protocols. First, relatively homogeneous areas were selected using the LabelVoxel module, which selects all pixels of a brightness that falls within a specified range of values. Areas such as the exterior of the animal, the interior of the stomach, and the tubules of the hepatopancreas were segmented in this way (all of these areas are uniformly black). Additional tissues were segmented with a mélange of semi-automated two- and three-dimensional (3D) selection tools, including the Magic Wand, Propagating Contour and Blowtool. Tissues such as the hepatopancreas and the stomach were segmented in this way, and were cleaned up manually using the Brush tool. The brain and whole-body crayfish were segmented using this same sequence of protocols. Delineation of the boundaries of each structure was accomplished with the aid of atlases of crayfish anatomy (Huxley, 1880; Ringel, 1924; Fretter and Graham, 1976; Sandeman et al., 1992; Vogt, 2002). The boundaries of most tissues were obvious. In cases where they were not, we used criteria outlined in other MRI atlas projects (Dhenain et al., 2001) and anatomical atlases (Brune et al., 1999) to determine exact boundaries. These criteria included (i) the shape of the structure in three dimensions (comparisons with adjacent slices in the sagittal, coronal, and transverse orientations), (ii) the position of surrounding tissues, and (iii) comparison with position of the structure in existing atlases and dissections. Only structures that could be clearly identified were included in the model. 3D surface models were automatically generated from labeled slices using the SurfaceGenerator module in Amira™. Individual segments of the movies were produced with Amira™ and subsequently assembled using Adobe® Premier® 6.5 on a personal computer.

Results

Conventional MRI

We initially explored the possibility of imaging anatomical structures of an adult female crayfish with conventional MRI (Fig. 1). The animal was immobilized in a round centrifuge tube and subsequently imaged inside a 4.7 Tesla horizontal bore magnet with a quadrature birdcage RF coil typically used for small rodents. A multi-slice spin-echo sequence was used with a number of different arbitrarily selected MR parameters. Parameters that offered the best contrast and visibility of tissue were then chosen.

Fig. 1A shows a representation of the external morphology of the crayfish reconstructed from MRI images using data processing software on a PC. Internal anatomical structures (Fig. 1B) were identified with aid of published reports of crayfish anatomy (Fretter and Graham, 1976; Vogt, 2002) and include the stomach, eggs, gut, hepatopancreas (where digestive enzymes are synthesized and nutrients are absorbed and metabolized) and antennal glands (the main excretory organ).

The limitations of this approach were quickly recognized, however. Certain anatomical structures were entirely undetectable in the acquired images (e.g. the brain and ventral nerve cord) or could not be distinguished because of overlapping borders due to low contrast (e.g. most muscle tissues and the cardio-vascular system). Reconstructing internal anatomical details of different organs (e.g. the hepatopancreas) was impossible. Thus, when using an animal with unknown MRI history, images acquired in one session using an arbitrary set of MR parameters that were determined after some experimentation only provide a general overview of the morphology of a limited number of structures. Sampling the images at higher resolution requires much longer scanning times to achieve the same signal-to-noise ratio (SNR) and does not increase the contrast between tissues. Performing several imaging sequences at different weightings (e.g. T_1, PD, T_2) to highlight different tissues in subsequent sessions – the traditional solution to the problem – also substantially increases the imaging time and makes the post-processing reconstruction into 3D models more difficult and time consuming.

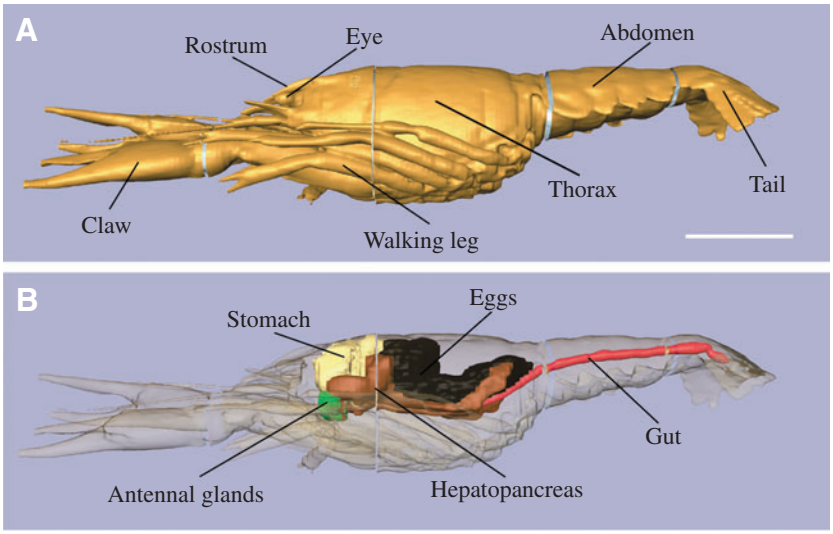

Fig. 1. The external and internal morphology of a live crayfish reconstructed from images acquired with conventional MRI. (A) The body surface of an adult female crayfish (mass 28.8 g) reconstructed with digital 3D processing. The animal was imaged in five partitions of 40 slices each to avoid signal drop-off. Scale bar: 2 cm. (B) Internal anatomy of the same animal. Imaging parameters: T_R=1.5 s, T_E=12.5 ms; matrix dimensions: 256×128, field of view=4 cm×4 cm, number of averages=8, slice thickness, 1000 µm; voxel size, 156×312×1000 µm; acquisition time (total), 2.1 h.

Manganese-enhanced MRI

We tested the ability of ionic Mn^{2+} to act as a contrast agent that allows us to identify anatomical structures in crayfish that were undetectable or undistinguishable with conventional MRI. The following two areas of biological interest were explored: (1) the brain (or supraesophageal ganglion), because active neurons reportedly accumulate Mn^{2+} and because the small size of the brain (~3 mm×1.5 mm×2 mm) appeared to be especially challenging, and (2) the foregut (and surroundings), because of the variety of complex structures that are part of it and because the most detailed anatomical descriptions of the crayfish stomach available were published many years ago (Huxley, 1880; Ringel, 1924; Fretter and Graham, 1976).

Animals were cannulated in the pericardial sinus with silica tubing for systemic injection of $MnCl_2$. The combination of Mn^{2+} concentration and MR parameters that generated the greatest improvement of contrast and overall signal intensity in our areas of interest was determined by varying the administered doses of $MnCl_2$ and changing T_R and T_E in a series of short, low-resolution scans. Each of these scans only took a few minutes and was composed into a matrix (with variation in $MnCl_2$ doses on the *x*-axis and variations of T_R and T_E on the *y*-axis) that was subsequently reviewed. This allowed us to select combinations that produced the maximum effect of Mn^{2+} as a contrast agent for imaging the central nervous system and thoracic region of crayfish. In accordance with earlier descriptions of the paramagnetic properties of Mn^{2+}, we found that selecting T_R and T_E values (T_R=1.5 s, T_E=17.6 ms) in the range of T_1-weighted imaging produced the best results. Having established the most suitable imaging parameters, we administered 60 µl of a solution of 120 mmol l^{-1} $MnCl_2$ in saline for imaging of the brain and thorax (Fig. 2). Injections took place inside the magnet so that the effects of Mn^{2+} could be demonstrated in the exact same location in the same animal. Single slices from transverse sections through the animal's head before and after $MnCl_2$ injection revealed dramatic differences (Fig. 2A): the brain is basically undetectable before the injection but becomes clearly visible, situated between the bilateral bases of the antennae (An) and below the rostrum (Ro), a few minutes after the injection. At this dose, the enhancement begins less than 7 min after the injection. This enhancement peaks after approximately 30 min and remains unchanged for the next several hours. Re-imaging the animals 48 h after the initial experiment showed that the amount of Mn^{2+} (as measured by signal intensity of affected tissues) had diminished, and 6 days later it was completely eliminated.

Retaining the same imaging parameters and dose of $MnCl_2$ that was systemically administered within the magnet, transverse sections through the thoracic area of the crayfish also revealed better contrast between tissues and greater overall signal intensity after Mn^{2+} injection (Fig. 2B). Specifically, the boundaries around the stomach (St) and around the two lobes of the hepatopancreas (He) are more distinct, and tissues inside and between the gill chambers (GC) are more pronounced. Water (Wa) surrounding the forward directed walking legs (WL) shows slightly increased signal intensity indicating that the animals started the excretion of Mn^{2+}.

Interestingly, we found that after injection of Mn^{2+}, the signal intensity is selectively enhanced in certain tissues but appears suppressed in others (around the brain, outside the hepatopancreas, inside the walking legs). This previously described effect of the contrast agent (Li et al., 2004) is particularly developed after injection of larger amounts of $MnCl_2$ and can additionally improve contrast between areas of interest and the surrounding tissue.

High-resolution scan of the brain

Since a slight suppression of signal intensity in tissues surrounding the brain (thus enhancing brain contrast) was observed using 60 µl of a 120 mmol l^{-1} $MnCl_2$ solution (Fig. 2A), we decided to exploit this effect for a high-resolution scan of the brain, and injected the animals with the highest possible dose of $MnCl_2$ (100 µl/120 mmol l^{-1}) that was still low enough not to cause any unusual behavior indicative of toxication. To ensure even distribution of the contrast agent throughout the body and to prevent pooling, which was occasionally observed when the contrast agent was administered inside the scanner, we injected the $MnCl_2$ 1 h

before imaging, placed the crayfish in water-filled tanks and evoked locomotive behavior during that time.

Fig. 3 and Movie 1 ('brain' in supplementary material) show an anatomical 3D model of the crayfish brain and its external and internal structures reconstructed from images collected at a resolution of 68 µm×68 µm×250 µm. The animal was injected 1 h prior to imaging, previously established T_R and T_E values were used, and the total acquisition time was 20.5 h. The model incorporates the three separate regions of the brain that have been previously described and reconstructed from histological sections (Sandeman et al., 1992). A frontal view with the exoskeleton made transparent on the right (Fig. 3A) shows the protocerebrum, which includes the optic ganglia, lamina (La) and medullae (Me; consisting of medulla externa, medulla interna and medulla terminalis), which are located in each of the two eyestalks (Est) as well as the optic nerves (ON). The deutocerebrum contains the anntenular nerves (AntN) projecting into the bases of the antennules (Ant), and the tritocerebrum includes the antennal nerves (AnN) projecting into the bases of the antennae (An). These identified structures are shown again in Fig. 3B without the surrounding exoskeleton. Due to the high spatial resolution of the acquired images, internal structures of the main brain area (colored white in Fig. 3A,B) were also readily identified and are displayed in Fig. 3C. Separate regions of the brain such as the olfactory (OL) and accessory lobes (AL), several cell clusters (6,10,17), the antennal neuropiles (AnP), the esophageal connectives (EC) and a large artery (Ar) can be distinguished from the more central areas (white color). Movie 1 ('brain' in supplementary material) additionally illustrates the 3D nature of this brain model.

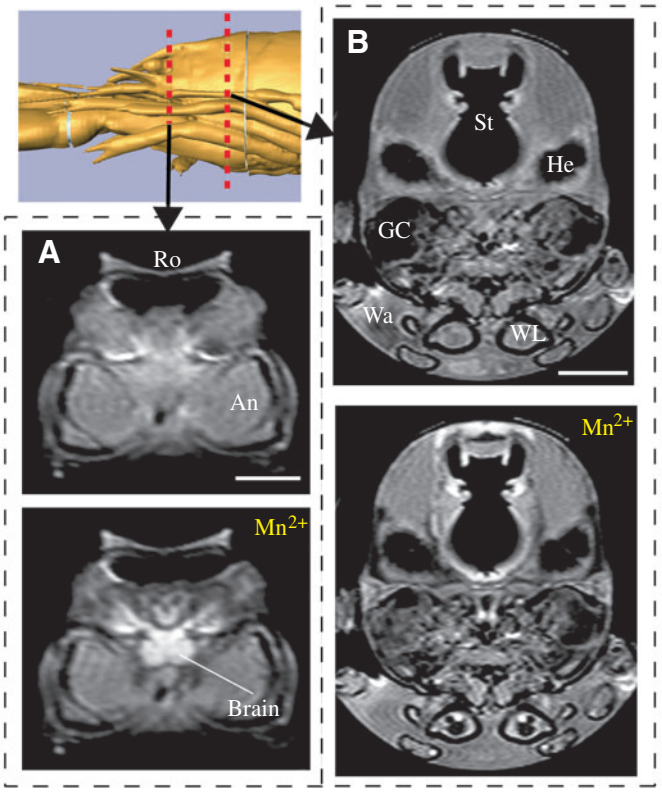

Fig. 2. The effects of systemically administered Mn^{2+} as a signal and contrast enhancer in crayfish. (A) Single transverse slices through the head of an adult male crayfish (mass 33.5 g) illustrate the difference in contrast before (top) and 32 min after (bottom) injection of 60 µl of a 120 mmol l^{-1} $MnCl_2$ solution. The brain is undetectable before injection but exhibits the strongest signal and appears below the rostrum (Ro) and between the bases of the bilateral antennae (An) afterwards. Scale bar, 4 mm. (B) Single transverse slices through the thorax of an adult male crayfish (mass 34.0 g), before (top) and 32 min after (bottom) injection of 60 µl of a 120 mmol l^{-1} $MnCl_2$ solution. Boundaries around the air-filled stomach (St) are more distinct and contrast around and within different areas, e.g. hepatopancreas (He) and gill chamber (GC) is clearly enhanced after injection. The walking legs (WL) are pointing forward and are surrounded by water (Wa) in the tube. Scale bar, 6 mm. Imaging parameters: T_R=1.5 s, T_E=17.6 ms; matrix dimensions: 256×128, field of view=5.12 cm×5.12 cm, number of averages=2, slice thickness, 1000 µm; voxel size, 200×400×1000 µm; acquisition time (each), 6.4 min. Inset: Red lines indicate the position of the transverse slices through the head and thorax, as shown in A and B, respectively.

High-resolution scan of the thorax

We also imaged the part of the thorax that contains the crayfish stomach at high resolution (200 µm×200 µm×200 µm). The crayfish was injected with 60 µl of a 120 mmol l^{-1} $MnCl_2$ solution 1 h prior to imaging. The previously established T_R and T_E values were used and the total acquisition time was 12.5 h. Digital post-processing allowed the reconstruction of this body part into yet another anatomical 3D model (Fig. 4; Movie 2 ('thorax' in supplementary material).

Fig. 4A and B show an angled and side view, respectively, of prominent structures within the imaged body region. Reconstructed from MRI data using post-processing software, we were able to identify and label ventral (VA) and antennary arteries (AnA), antennal glands (AG), the anterior part of both lobes of the hepatopancreas (He) and the foregut, including the stomach (St) and esophagus (Es). Groups of muscles that were also identified are not displayed for reasons of clarity. In Fig. 4B, adding transparency to the hepatopancreas (He) reveals the hepatopancreatic tubules (HeT) within and their connection to the stomach, while a cut through the antennal gland allows visualization of the interior of the antennal glands (iAG; consisting of coelomosac, labyrinth and nephridial tubule) that is surrounded by the bladder (Bl). The complex internal anatomy of the stomach can also be visualized in sagittal and coronal sections (Fig. 4C,D): both compartments of the stomach can be seen together with their internal anatomical structures devoted to different stages of digestion. The anterior cardiac stomach (CSt) includes the gastric mill with two lateral teeth (LT) and one medial tooth (MT) that grind the food as well as the ventrolateral cardiac filter (VCF). The food is then transported past the cardio-pyloric valve (CpV) into the pyloric stomach (Pst) where it is filtered again and digestible and indigestible material is separated. Digestible matter passes into the hepatopancreatic tubules while

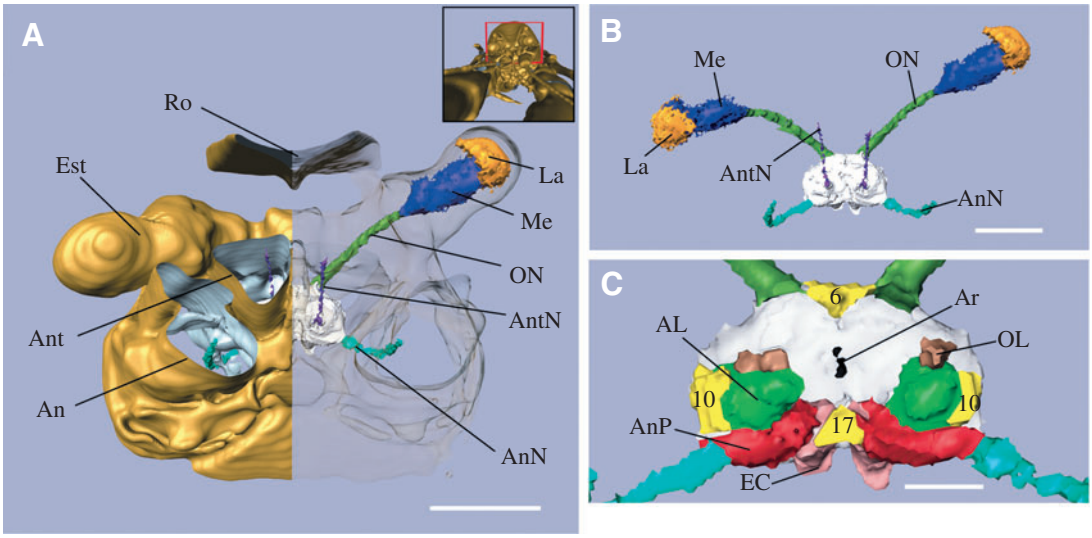

Fig. 3. The anatomy of the crayfish brain and its internal subdivisions. (A) 3D model of the crayfish brain (white) shown inside the exoskeleton (made transparent on the right) in a frontal view. Optic nerves (ON) that project into the eyestalks (Est) and the optic ganglia, lamina (La) and medullae (Me; consisting of medulla externa, medulla interna and medulla terminalis) within the eyestalks, are shown. Antennular (AntN) and antennal (AnN) nerves that project into the bases of the antennules (Ant) and antennae (An), respectively, are also displayed. Ro, rostrum. Scale bar, 4 mm. Inset: Red box indicates the area displayed beneath in the enlargement. (B) The brain and nerves shown without the exoskeleton. Scale bar, 3 mm. (C) Enlargement of the deuto- and tritocerebrum. Identified and displayed structures are the olfactory (OL) and accessory (AL) lobes, the antennal neuropils (AnP), a large artery (Ar), several prominent cell clusters (6, 10, 17) and the esophageal connectives (EC). Scale bar, 1 mm. Data in A–C were reconstructed from images acquired from the same crayfish (mass 37.9 g) that had been injected with 100 µl/120 mmol l^{-1} $MnCl_2$ prior to scanning at T_R=1.5 s, T_E=17.6 ms; matrix dimensions: 512×512, field of view=3.5 cm×3.5 cm, number of averages=96, slice thickness, 250 µm; voxel size, 68×68×250 µm; acquisition time (total), 20.5 h.

indigestible matter is transferred through the dorsal valve (DV), which spans the midgut, into the hindgut. Movie 2 ('thorax' in supplementary material) additionally illustrates the 3D nature of this model.

Discussion

We found that Mn^{2+} can act as a potent contrast agent for MRI in an aquatic invertebrate. After injection into the animal, the Mn^{2+} ions are quickly distributed and differentially accumulate in soft tissues to boost the overall signal intensity and significantly enhance contrast. Higher overall signal intensity ensures achieving better SNR and therefore the potential for higher spatial resolution within the same amount of acquisition time. An improved contrast-to-noise ratio permits structures of interest to be separated without having to vary the MR parameters across multiple imaging sessions. We found that systemic injection of one dose of contrast agent is sufficient to enhance signal and contrast in two different anatomical areas (i.e. the brain and thorax). However, higher doses of Mn^{2+} can cause signal suppression in some tissues, an effect that can be utilized to improve contrast when imaging certain areas such as the brain. We also found that images captured from Mn^{2+}-injected animals revealed anatomical details that were still undetectable after testing different sets of imaging parameters with conventional MRI (e.g. fine structures of the nervous tissue, boundaries around the stomach). As a result, Mn^{2+}-injected crayfish only need to endure one imaging session, which is sufficient to obtain the information required for subsequent anatomical reconstruction. The only preparatory procedure is to determine the optimal combination between the concentration of the injected agent and the MR parameters. Since Mn^{2+} is a T_1-relaxation agent, the MR parameters that need to be tested are constrained within a narrow range and can be determined in few short sessions. Thereafter, the acquisition time needed for the desired spatial resolution mainly depends on the magnetic field strength and the size and type of the RF coil used. Our results show that application of Mn^{2+} as a contrast agent yields satisfactory results by use of a medium-strength magnetic field and a regular RF birdcage coil typically used for imaging rodents.

Crayfish are surprisingly well suited for manganese-enhanced MRI because they tolerate Mn^{2+} injections well, quickly distribute the contrast agent throughout the body, and can eliminate it after a few days. This allows injection of the Mn^{2+} when the animal is inside or outside the magnet and imaging the same animal before and after injection as well as re-imaging it after the initial dose of the contrast agent has cleared.

The fast and extensive uptake of Mn^{2+} by the nervous tissue seen in our study opens up the possibility that Mn^{2+} could also be used to identify patterns of neural activity in the brains of crayfish, in a process analogous to procedures already established in rodents (Lin and Koretsky, 1997). Since crayfish are a model system for neurobiologists and provide easy access for intracellular investigations, this is clearly an exciting possibility. The animals could be injected with $MnCl_2$ while freely behaving and Mn^{2+} would then be expected to accumulate in brain areas that were active during the behavioral performance. Preliminary experiments in this direction using electrical stimulation to the olfactory organs have been promising (Herberholz et al., 2003).

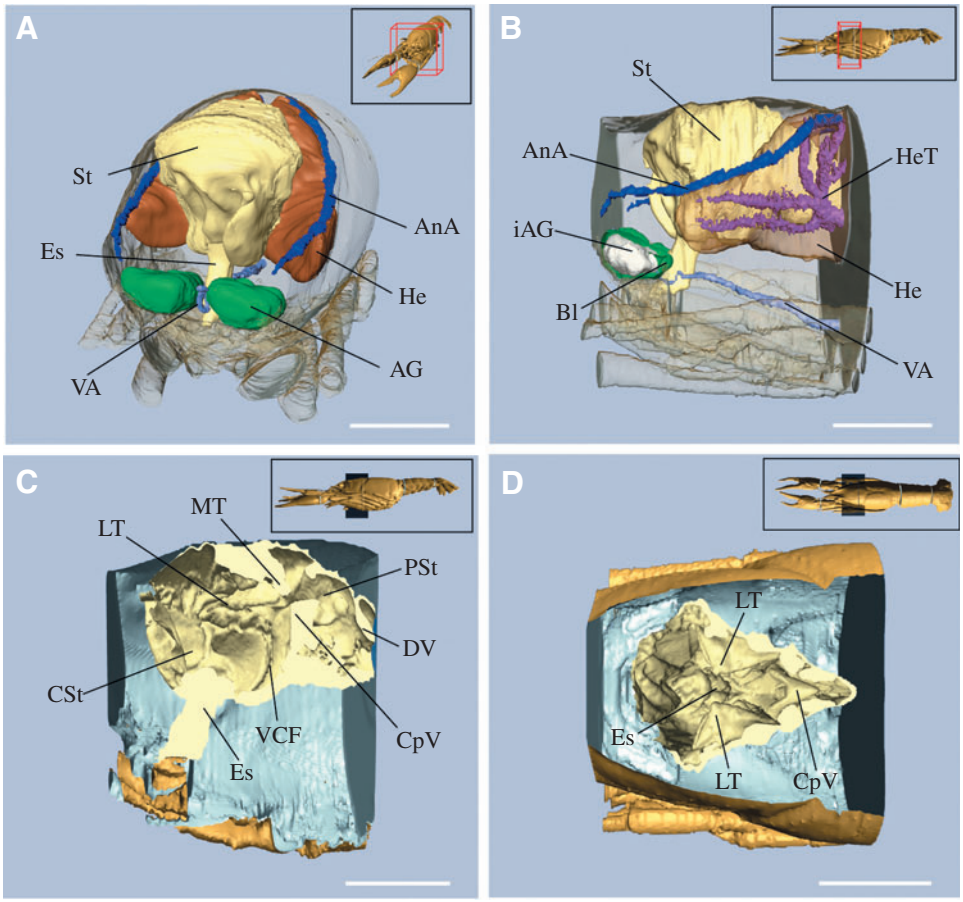

Fig. 4 The anatomy of the thoracic region and stomach of crayfish. (A) Angled view of a 3D model reconstructed from MRI data. The anatomical structures identified and displayed within the thoracic region are the bilateral antennary arteries (AnA), the ventral artery (VA), the antennal glands (AG), the anterior part of both lobes of the hepatopancreas (He) and the foregut, including the stomach (St) and esophagus (Es). The exoskeleton was made transparent for better illustration. (B) A side view of the same model. Cutaway of antennal gland and added transparency to the hepatopancreas reveal internal structures. The bladder (Bl) almost completely encloses the remaining tissue (iAG) of the antennal glands. The hepatopancreatic tubules (HeT) inside the hepatopancreas and the duct that connects them to the stomach can also be seen. Insets in A and B: Red boxes indicate the area displayed beneath in the enlargements. (C) Sagittal section of the stomach. The internal structures identified and displayed within the foregut are the esophagus (Es), the cardiac stomach (CSt), the lateral (LT) and medial tooth (MT), the ventrolateral cardiac filter (VCF), the cardio-pyloric valve (CpV), the pyloric stomach (PSt) and the dorsal valve (DV). (D) Coronal section of the (cardiac) stomach. Identified and displayed structures are the lateral teeth (LT), the esophagus (ES) and the cardio-pyloric valve (CPV). The external tissue surrounding the interior of the stomach is displayed as a uniform structure in bright yellow color. Other organs were removed for means of clarity. Insets in C and D: Dark planes indicate the positions at which the portions of the crayfish displayed beneath in the enlargements were cut open. All scale bars, 1 cm. Data in A–D were reconstructed from images acquired in the same crayfish (mass 31.8 g) that was injected with 60 µl of a 120 mmol l^{-1} $MnCl_2$ solution and scanned at T_R=1.5 s, T_E=17.6 ms; matrix dimensions: 256×256, field of view=5.12 cm×5.12 cm, number of averages=20, slice thickness, 200 µm; voxel size, 200×200×200 µm; acquisition time (total), 12.5 h.

The tendency of Mn^{2+} to accumulate differentially in soft tissues qualifies it as a useful contrast agent for most anatomical structures. We found that systemic injection of $MnCl_2$ into a crayfish increased contrast between complex structures sufficiently to enable reconstruction of detailed 3D models from the images. Anatomical reconstructions were accomplished with the aid of atlases of crayfish stomach anatomy (Huxley, 1880; Ringel, 1924; Fretter and Graham, 1976) and previously published descriptions of the brain anatomy (Sandeman et al., 1992) obtained from histological sections. While histology and electron microscopy provide higher spatial resolution than our images, these techniques require destructive procedures and cannot provide a natural representation of the living animal.

We speculate that only minor modifications are required to make manganese-enhanced MRI applicable for quickly imaging the anatomy of many other live invertebrates, including those of smaller size. The optimal dose of the contrast agent has to be established, the administration into smaller subjects may be more challenging, and immobilization techniques to prevent motion artefacts during imaging must be explored. Overall, these preparations are negligible when compared to the outcome. Tracking the anatomical and morphological changes during development or metamorphosis in the same animal, comparing differences between larval and adult forms, measuring the effects of drug application or genetically induced modifications of organs and body tissues, or simply adding knowledge about the anatomy of model systems used in various disciplines, can more easily be accomplished with this technique. In summary, it provides a large number of biologists who have an interest in invertebrate anatomy with a more effective and less time-consuming imaging tool than conventional MRI and presents an exciting alternative to other more invasive techniques.

We would like to thank Bernadette Loncke, Drs. Manfred Schmidt and Robert Long for their help, and also Dr Barbara Beltz (Wellesley College, MA, USA) for her suggestion to examine crustaceans with MRI. This work was supported by the STC Program of the NSF under Agreement No. IBN-

9876754 (J.H.), the Georgia Research Alliance, and NIH grants R01 EB002009 (X.H.) and R01 NS26457 (D.H.E.).

References

Aoki, I., Ebisu, T., Tanaka, C., Katsuta, K., Fujikawa, A., Umeda, M., Fukunaga, M., Takegami, T., Shapiro, E. M. and Naruse, S. (2003). Detection of the anoxic depolarization of focal ischemia using manganese-enhanced MRI. *Magn. Res. Med.* **50**, 7-12.

Baden, S. P., Eriksson, S. P. and Gerhardt, L. (1999). Accumulation and elimination kinetics of manganese from different tissues of the Norway lobster *Nephrops norvegicus* (L.). *Aquat. Toxicol.* **46**, 127-137.

Baden, S. P. and Neil, D. M. (1998). Accumulation of manganese in the haemolymph, nerve and muscle tissue of *Nephrops norvegicus* (L.) and its effect on neuromusculator performance. *Comp. Biochem. Physiol.* **119**, 351-359.

Benveniste, H. and Blackband, S. (2002). MR microscopy and high resolution small animal MRI: applications in neuroscience research. *Progr. Neurobiol.* **67**, 393-420.

Brune, R. M., Bard, J. B., Dubreuil, C., Guest, E., Hill, W., Kaufman, M., Stark, M., Davidson, D. and Baldock, R. A. (1999). A three-dimensional model of the mouse at embryonic day 9. *Dev. Biol.* **216**, 457-468.

Dhenain, M., Ruffins, S. W. and Jacobs, R. E. (2001). Three-dimensional digital mouse atlas using high-resolution MRI. *Dev. Biol.* **232**, 458-470.

Fretter, V. and Graham, A. (1976). Crustaceans. In *A Functional Anatomy of Invertebrates*, pp. 280-362. Academic Press, New York.

Herberholz, J., Mims, C. J., Zhang, X., Hu, X. and Edwards D. H. (2003). Manganese-enhanced MRI of the crayfish brain. *Soc. Neurosci. Abstr.* **29**, 270.5.

Huxley, T. H. (1880). *The Crayfish. An Introduction to the Study of Zoology.* New York: D. Appleton and Company. 371p.

Li, S. K., Jeong, E. K. and Hastings, M. S. (2004). Magnetic Resonance Imaging study of current and ionic delivery into the eye during transscleral and transcorneal iontophoresis. *Invest. Ophthalmol. Vis. Sci.* **45**, 1224-1231.

Lin, Y. J. and Koretsky, A. P. (1997). Manganese ion enhanced T_1-weighted MRI during brain activation: an approach to direct imaging of brain function. *Magn. Res. Med.* **38**, 378-388.

Morita, H., Ogino, T., Seo, Y., Fujiki, N., Tanaka, K., Takamata, A., Nakamura, S. and Murakami, M. (2002). Detection of hypothalamic activation by manganese ion contrasted T_1-weighted magnetic resonance imaging in rats. *Neurosci. Lett.* **326**, 101-104.

Pautler, R. G., Silva, A. C and Koretsky, A. P. (1998). In vivo neuronal tract tracing using manganese-enhanced magnetic resonance imaging. *Magn. Reson. Med.* **40**, 740-748.

Pautler, R. G., Mongeau, R. and Jacobs, R. E. (2003). In vivo trans-synaptic tract tracing from the murine striatum and amygdala utilizing manganese enhanced MRI (MEMRI). *Magn. Res. Med.* **50**, 33-39.

Ringel, M. (1924). Zur Morphologie des Vorderdarmes (Schlund und Magen) von *Astacus fluviatilis* (*Potamobius astacus* L.). *Z. wiss. Zool.* **123**, 498-554.

Runge, V. M. (2000). Safety of approved MR contrast media for intravenous injection. *J. Magn. Res. Imaging* **12**, 205-213.

Sandeman, D., Sandeman, R., Derby, C. and Schmidt, M. (1992). Morphology of the brain of crayfish, crabs, and spiny lobsters – a common nomenclature for homologous structures. *Biol. Bull.* **183**, 304-326.

Vogt, G. (2002). Functional anatomy. In *Biology of Freshwater Crayfish* (ed. D. M. Holdich), pp. 53-151. Oxford, UK: Blackwell Science.

Weinmann, H. J., Ebert, W., Misselwitz, B. and Schmitt-Willich, H. (2003). Tissue-specific MR contrast agents. *Eur. J. Radiol.* **46**, 33-44.